ISSN 1063-7737, Astronomy Letters, 2015, Vol. 41, No. 5, pp. 211–224. © Pleiades Publishing, Inc., 2015.
Original Russian Text © A.A. Solov'ev, E.A. Kirichek, 2015, published in Pis'ma v Astronomicheskiĭ Zhurnal, 2015, Vol. 41, No. 5, pp. 234–247.

Magnetohydrostatics of a Vertical Flux Tube in the Solar Atmosphere: Coronal Loops, a Model of a Ring Flare Filament

A. A. Solov'ev* **and E. A. Kirichek**

Pulkovo Astronomical Observatory, Russian Academy of Sciences, Pulkovskoe sh. 65, St. Petersburg, 196140 Russia

Received September 12, 2014

Abstract—The magnetohydrostatic theory of a twisted magnetic flux tube (rope) immersed in a realistic solar atmosphere is presented in a closed analytical form for the first time. General formulas that allow the equilibrium plasma density, pressure, and temperature distributions inside an axisymmetric vertical flux tube to be calculated from its magnetic structure, which is assumed to be known (fixed), have been derived. An analytical model of the external hydrostatic medium free of a magnetic field, the solar atmosphere, where the temperature profile of the semi-empirical tabulated Avrett–Loeser model is used, has been constructed. The distribution of plasma parameters in a twisted magnetic flux tube at small deviations of its internal magnetic structure from the force-free one has been calculated as an example of applying the general theoretical formulas. Since the tube cross section does not change with height, the constructed model can be applied to describe the vertical parts of coronal loops. It has been found that the plasma density in the magnetic flux tube rises when the field twisting exceeds the force-free level and falls with decreasing field twisting compared to the force-free level. This property of a twisted magnetic flux tube is of fundamental importance for justifying the mechanism of flare energy release in magnetic flux ropes. A model of a flare in a ring chromospheric configuration is considered.

DOI: 10.1134/S1063773715050072

Keywords: *magnetohydrostatics, solar atmosphere, coronal loops.*

1. INTRODUCTION

Many manifestations of solar activity on the surface of the Sun are associated with long-lived magnetic structures whose lifetime exceeds considerably the characteristic time it takes for a magnetohydrodynamic equilibrium to be established in the system. These include, for example, sunspots, quiescent prominences, chromospheric filaments, coronal loops, coronal holes, etc. The magnetohydrostatic approximation can be used with good reason to describe such structures (Parker 1979; Priest 1982; Low 1975, 1980, 1982, 1985; Tsinganos 1981; Obridko and Solov'ev 2011; Solov'ev and Kirichek 2011, 2014; etc.). Interestingly, even in such a relatively fast process as the solar flare, the flare filament (unless it flies out immediately into the corona and interplanetary space in the form of a coronal mass ejection, CME) may be considered as a quasi-static structure. Indeed, a flare typically lasts 10–20 min and occasionally much longer (up to several hours), while the characteristic time it takes for an equilibrium to be established in the system (along the cross section and the radius of curvature) is $\tau_a \approx aV_\mathrm{A}^{-1}$ and $\tau_R \approx RV_\mathrm{A}^{-1}$, respectively, where a is the cross-sectional radius of the magnetic flux rope, R is the radius of curvature of its magnetic axis, and V_A is the Alfvén speed. Typical estimates for these quantities can be $a \approx 0.5 \times 10^9$ cm and $R \approx 1 \times 10^{10}$ cm, while V_A will be several units $\times 10^8$ cm s^{-1} if we take the mean gas density in the filament to be equal to the chromospheric one at the level of the transition region ($\approx 10^{-13}$ g cm^{-3}) and the magnetic field in the flare chromospheric filament to have a strength no less than 300 G (to provide sufficient energetics of the entire flare). Then, $\tau_a \approx aV_\mathrm{A}^{-1} < 5$ s and $\tau_R \approx RV_\mathrm{A}^{-1} < 100$ s, which is much shorter than the flare duration. In particular, this means that the flare magnetic filament both in its initial state and during the violent energy release in it may be considered on the whole as a quasi-static object, i.e., it may be assumed that evolving relatively rapidly with time due to large Ohmic losses, the system nevertheless passes a continuous sequence

*E-mail: solov@gao.spb.ru

of equilibrium states, because the characteristic time of change in its physical parameters in the flare process is appreciably longer than the characteristic Alfvén time (Solov'ev 2012, 2013; Solov'ev and Murawski 2014).

In addition, the outward appearance of many long-lived solar structures often allows quite a justified assumption about the presence of a shift (translational) or axial symmetry in them to be made. In these cases, the problem of describing the equilibrium of such systems is simplified sharply, although it by no means becomes trivial in view of the nonlinearity of the magnetic force. In spite of the fact that an enormous number of works are devoted to investigating the magnetostatic equilibrium of solar magnetic structures, many unsolved problems still remain. Thus, for example, the fact that the long-lived coronal loops (especially their side branches or "feet") do not change noticeably their cross-sectional radius all the way from the footpoints almost to the loop tops located high in the corona is a puzzle. Recently, Gent et al. (2014) has presented a model of a vertical magnetic flux tube where the magnetic field distribution obeys a scaling law as a considerable step forward in the theory of coronal loops. The specific model proposed by the authors is not an equilibrium one; there is no balance of forces (the pressure gradient, the magnetic force, and the gravity force) in the chromospheric part of such a tube. The authors see a way out of the situation in the fact that alluding to the complex structure of chromospheric layers, they admit the existence of some additional forces of an unknown physical nature that allegedly provide an equilibrium of the configuration they constructed. Such an approach flatly contradicts the basic laws of physics and is of no scientific interest. The problem of the magnetostatic theory of coronal magnetic loops remains an unsolved and very topical problem of solar physics.

In this paper, we propose a closed analytical theory of the equilibrium of a vertical magnetic flux tube with axial symmetry, derive general formulas that allow the pressure and density in such a configuration to be calculated from a specified magnetic structure, and consider specific examples of their application.

The paper has the following structure. In Section 2, we provide the basic equations and formulate the problem. The formulas for the plasma pressure and density in an equilibrium axisymmetric configuration are derived in Section 3. An analytical model of the external medium, a hydrostatic solar atmosphere, is presented in Section 4. A specific example of a magnetic structure with a field distribution close to the force-free state is considered in Section 5. The mechanism of energy release in twisted magnetic flux tubes (ropes) is analyzed in Section 6. A model of a ring flare filament is presented in Section 7. The boundary conditions are analyzed in Section 8. Our conclusions are briefly formulated in the Conclusions.

2. THE MAGNETOHYDROSTATIC EQUATIONS AND FORMULATION OF THE PROBLEM

Consider the magnetohydrostatic problem of calculating the structure of the magnetic field and plasma for a straight vertical axisymmetric magnetic flux tube in a plane-parallel equilibrium atmosphere in the presence of a uniform gravity field $\mathbf{g}$. Axial symmetry suggests invariance with respect to arbitrary rotations of the system around the filament axis. Let this be the vertical z axis in cylindrical coordinates r, φ, and z; we will measure the distances along this axis upward from the photospheric level. The gravity force is expressed as $\mathbf{F}_g = -\rho g(z)\mathbf{e}_z$, where ρ is the gas density, and the system of magnetohydrostatic equations will take the form

$$\nabla P + (4\pi)^{-1}[\mathrm{curl}\,\mathbf{B}\times\mathbf{B}] - \rho g(z)\mathbf{e}_z = 0, \quad (1)$$

$$\mathrm{div}\,\mathbf{B} = 0, \quad (2)$$

$$P = \rho\Re T\mu^{-1}. \quad (3)$$

The notation is traditional: $\mathbf{B}$ is the magnetic field strength, P and T are the gas pressure and temperature, respectively, and μ is the mean molar mass of the gas. Equations (1), (2), and (3) describe, respectively, the balance of forces in the equilibrium system, the solenoidal nature of the magnetic field, and the state of an ideal gas. System (1)–(3) is incomplete: there is no energy transfer equation in it; therefore, some of the dependences should be specified additionally in magnetohydrostatics. In the presence of axial symmetry, system (1)–(3) is reduced to the following triplet of equations (Low 1975):

$$\frac{\partial^2 A(r,z)}{\partial r^2} - \frac{1}{r}\frac{\partial A}{\partial r} + \frac{\partial^2 A(r,z)}{\partial z^2} = -\frac{1}{2}\frac{d\Omega^2(A)}{dA} - 4\pi r^2\frac{\partial P(A,z)}{\partial A}, \quad (4)$$

$$\rho(r,z)g(z) = -\frac{\partial P(A,z)}{\partial z}, \quad (5)$$

$$T(r,z) = \frac{\mu}{\Re}\frac{P(r,z)}{\rho(r,z)}. \quad (6)$$

Here, $A(r,z) = \int_0^r B_z(r,z)rdr$ is the flux of the vertical magnetic field through a horizontal circle of radius r (without the factor 2π), $\Omega(r,z) = \frac{4\pi}{c}\int_0^r j_z rdr = rB_\varphi(r,z)$ is the vertical electric current through the same horizontal circle. The geometric shape of the magnetic field lines in projection onto

the (r, z) plane is given by the condition $A(r, z) =$ const. Equation (5) describes the hydrostatic equilibrium of the gas along a magnetic field line. The poloidal field components are defined via the function A by the relations

$$B_z = \frac{1}{r}\frac{\partial A}{\partial r}, \quad B_r = -\frac{1}{r}\frac{\partial A}{\partial z}, \tag{7}$$

which automatically ensure the fulfilment of condition (2), while the electric current Ω in the presence of axial symmetry depends only on the magnetic flux $A(r, z)$: $\Omega = \Omega(A) = rB_\varphi$. Thus, the magnetic structure of the equilibrium configuration is defined to a crucial extent by the flux function $A(r, z)$. Owing to the presence of a potential external field $\mathbf{g}$, the gas pressure on the right-hand side of Eq. (4), in contrast to the well-known Grad–Shafranov equation (Shafranov 1957; Grad 1960), depends not only on the magnetic flux A but also on the coordinate z. This important fact allows us to integrate Eq. (4) over the variable A and to express the gas pressure in terms of the functions A, $\Omega(A)$, and their derivatives and then to find the gas density and temperature from Eqs. (5) and (6), respectively. Thus, based on the known magnetic structure of the equilibrium configuration, we can completely calculate the plasma distribution in it. Low (1980, 1982) was the first to come up with this idea. As an example, he considered only one very simple specific case where the above integration is performed easily, but he derived no general formulas for $P(r, z)$ and $\rho(r, z)$ and, subsequently, did not return to this problem. Shapovalov and Shapovalova (2003) solved the problem of obtaining the equilibrium plasma distributions in a magnetic configuration immersed in a specified external potential field and admitting some one-parameter group of motions of 3D Euclidean space in the most general covariant form. Explicit expressions for the gas pressure and density in equilibrium systems with translational, axial, or helical symmetry, respectively, can be derived from the formulas given in this paper using the Killing vector. In the case under consideration, we will restrict our analysis only to axisymmetric configurations and will derive a formula for the pressure by directly integrating Eq. (4), find the density as the corresponding partial derivative of the pressure according to Eq. (5) and the temperature from Eq. (6). For horizontal filaments of an arbitrary cross section with translational symmetry, general formulas for $P(r, z)$ and $\rho(r, z)$ were derived and used to construct the prominence model in Solov'ev (2010).

3. THE PLASMA PRESSURE AND DENSITY IN AN AXISYMMETRIC MAGNETIC FLUX TUBE

Let us integrate Eq. (4) with respect to the function A by considering z as a fixed parameter. We will begin the integration from some point r^* located far from the axis of our system to some arbitrarily chosen point inside the configuration where $A = A(r, z)$. The magnetic field at the remote point r^* is completely absent (or is an external potential field), while $P(r^*, z) \equiv P_{\rm ex}(z)$ is the hydrostatic gas pressure distribution in the external medium free of the magnetic field (this can also be the vertical pressure profile in a potential magnetic field that does not disturb the hydrostatic equilibrium). Integrating the equilibrium equation (4) by taking into account the fact that $dA = \frac{\partial A}{\partial r}dr + \frac{\partial A}{\partial z}dz = \frac{\partial A}{\partial r}dr$ because $dz = 0$, we obtain

$$-4\pi(P(r, z) - P_{\rm ex}(z)) = \int_{A^*}^{A}\left(\frac{\partial^2 A}{r^2\partial r^2} - \frac{\partial A}{r^3\partial r} + \frac{\partial^2 A}{r^2\partial z^2} + \frac{1}{2r^2}\frac{d\Omega^2(A)}{dA}\right)dA,$$

$$-4\pi(P(r, z) - P_{\rm ex}(z)) = \frac{\Omega^2}{2r^2} + \int_{r^*}^{r}\frac{\Omega^2}{r^3}dr + \int_{r^*}^{r}\frac{1}{r^2}\left(\frac{\partial^2 A}{\partial z^2} + \frac{\partial^2 A}{\partial r^2}\right)\frac{\partial A}{\partial r}dr - \int_{r^*}^{r}\frac{1}{r^3}\left(\frac{\partial A}{\partial r}\right)^2 dr.$$

Taking the integral containing the second derivative with respect to r by parts and replacing r^* by the infinity sign, we will obtain a formula to calculate the pressure:

$$P(r, z) = P_{\rm ex}(z) - \frac{1}{8\pi}\left[\frac{\Omega^2}{r^2} + \frac{1}{r^2}\left(\frac{\partial A}{\partial r}\right)^2 - 2\int_{r}^{\infty}\frac{\Omega^2}{r^3}dr - \int_{r}^{\infty}\frac{2}{r^2}\frac{\partial^2 A}{\partial z^2}\frac{\partial A}{\partial r}dr\right]. \tag{8}$$

To calculate the plasma density in the flux tube, we must find the corresponding partial derivative $\frac{\partial P(A, z)}{\partial z}$ in accordance with Eq. (5), while Eq. (8) gives a function of the form $P(r, z)$. Note that the following relations are valid for P, just as for any differentiable function:

$$\frac{\partial P(r, z)}{\partial z} = \frac{\partial P(A, z)}{\partial z} + \frac{\partial P(A, z)}{\partial A}\frac{\partial A}{\partial z}, \tag{9}$$

$$\frac{\partial P(r,z)}{\partial r}=\frac{\partial P(A,z)}{\partial A}\frac{\partial A}{\partial r}. \quad (10)$$

From Eq. (9) we have

$$\frac{\partial P(A,z)}{\partial z}=\frac{\partial P(r,z)}{\partial z}-\frac{\partial P(A,z)}{\partial A}\frac{\partial A}{\partial z}. \quad (11)$$

Here, the derivative $\frac{\partial P(A,z)}{\partial A}$ remains unknown on the right-hand side. To find it, we will use Eqs. (10) and (8):

$$\frac{\partial P(A,z)}{\partial A}\frac{\partial A}{\partial r}=\frac{\partial P(r,z)}{\partial r}$$
$$=-\frac{1}{4\pi}\frac{\partial}{\partial r}\left[\frac{\Omega^2}{2r^2}+\frac{1}{2r^2}\left(\frac{\partial A}{\partial r}\right)^2-\int\limits_r^\infty\frac{\Omega^2}{r^3}dr\right.$$
$$\left.-\int\limits_r^\infty\frac{1}{r^2}\frac{\partial A}{\partial r}\frac{\partial^2 A}{\partial z^2}dr\right]$$
$$=-\frac{1}{4\pi}\left[-\frac{\Omega^2}{r^3}-\frac{1}{r^3}\left(\frac{\partial A}{\partial r}\right)^2+\frac{\Omega}{r^2}\frac{\partial\Omega}{\partial A}\frac{\partial A}{\partial r}\right.$$
$$\left.+\frac{1}{r^2}\frac{\partial A}{\partial r}\frac{\partial^2 A}{\partial r^2}+\frac{\Omega^2}{r^3}+\frac{1}{r^2}\frac{\partial A}{\partial r}\frac{\partial^2 A}{\partial z^2}\right].$$

Hence, eliminating $\frac{\partial A}{\partial r}$, we will get $\frac{\partial P(A,z)}{\partial A}=\frac{1}{4\pi}\left[\frac{1}{r^3}\frac{\partial A}{\partial r}-\frac{\Omega}{r^2}\frac{\partial\Omega}{\partial A}-\frac{1}{r^2}\frac{\partial^2 A}{\partial r^2}-\frac{1}{r^2}\frac{\partial^2 A}{\partial z^2}\right]$. Next, using (11), we find

$$\frac{\partial P(A,z)}{\partial z}=\frac{\partial P_{\rm ex}(z)}{\partial z}-\frac{1}{4\pi}\frac{\Omega}{r^2}\frac{\partial\Omega}{\partial A}\frac{\partial A}{\partial z}-\frac{1}{4\pi}\frac{\partial}{\partial z}$$
$$\times\left[\frac{1}{2r^2}\left(\frac{\partial A}{\partial r}\right)^2-\int\limits_r^\infty\frac{\Omega^2}{r^3}dr-\int\limits_r^\infty\frac{1}{r^2}\frac{\partial A}{\partial r}\frac{\partial^2 A}{\partial z^2}dr\right]$$
$$-\frac{1}{4\pi}\frac{\partial A}{\partial z}\left[\frac{1}{r^3}\frac{\partial A}{\partial r}-\frac{\Omega}{r^2}\frac{\partial\Omega}{\partial A}-\frac{1}{r^2}\frac{\partial^2 A}{\partial r^2}-\frac{1}{r^2}\frac{\partial^2 A}{\partial z^2}\right]$$

or

$$\frac{\partial P(A,z)}{\partial z}=\frac{\partial P_{\rm ex}(z)}{\partial z}-\frac{1}{4\pi}\frac{\partial}{\partial z}$$
$$\times\left[\frac{\left(\frac{\partial A}{\partial r}\right)^2-\left(\frac{\partial A}{\partial z}\right)^2}{2r^2}\right.$$
$$\left.-\int\limits_r^\infty\frac{1}{r^2}\left(\frac{\Omega^2}{r}+\frac{\partial A}{\partial r}\frac{\partial^2 A}{\partial z^2}\right)dr\right]$$
$$+\frac{1}{4\pi r}\frac{\partial A}{\partial z}\frac{\partial}{\partial r}\left(\frac{1}{r}\frac{\partial A}{\partial r}\right).$$

Finally, the mass density distribution in the magnetic flux tube is

$$\rho(r,z)=\rho_{\rm ex}(z)+\frac{1}{4\pi g} \quad (12)$$
$$\times\left\{\frac{\partial}{\partial z}\left[\frac{\left(\frac{\partial A}{\partial r}\right)^2-\left(\frac{\partial A}{\partial z}\right)^2}{2r^2}-\int\limits_r^\infty\frac{\Omega^2}{r^3}dr\right.\right.$$
$$\left.\left.-\int\limits_r^\infty\frac{1}{r^2}\frac{\partial A}{\partial r}\frac{\partial^2 A}{\partial z^2}dr\right]-\frac{1}{r}\frac{\partial A}{\partial z}\frac{\partial}{\partial r}\left(\frac{1}{r}\frac{\partial A}{\partial r}\right)\right\}.$$

4. THE ANALYTICAL MODEL OF A HYDROSTATIC SOLAR ATMOSPHERE

The functions $P_{ex}(z)$ and $\rho_{ex}(z)$ in Eqs. (8) and (11) represent the background, the external medium, a hydrostatic solar atmosphere (photosphere, chromosphere, and corona) unaffected by the magnetic field. To calculate the pressure and density distributions inside the magnetic configuration, we must know these unperturbed functions. The solar corona may be considered with a good accuracy to be in a state of hydrostatic equilibrium by neglecting the influence of the solar wind up to heights of the order of one solar radius (Obridko and Solov'ev 2011). The situation with the chromosphere is much more complex; this layer is distinguished by pronounced inhomogeneity and dynamism (the phenomenon of chromospheric spicules with speeds of tens of km s^{-1} and heights up to 10–12 Mm, the supergranulation network, etc; the dynamic properties of the chromosphere are partly taken into account by the fact that the microturbulent component $0.5\rho V_{\rm turb}^2$ determined from the profiles of chromospheric lines is included in the gas pressure of the medium maintaining its vertical equilibrium). Nevertheless, to have a basis for quantitative calculations, semi-empirical static models at the levels from subphotospheric layers to tens of Mm in the corona have been proposed and widely used for many years as some averaged description of the "quiet" solar photosphere, chromosphere, and corona. The Vernazza–Avrett–Loeser (VAL) model (Vernazza et al. 1981) had been considered for a long time to be the main model of the solar chromosphere, transition region, and inner corona. The Avrett–Loeser (AL) model (Avrett and Loeser 2008) that superseded the VAL model is the latest and probably most reliable (to date) and worked-out one among such models (there is a detailed overview and analysis of the preceding works on modeling the chromosphere and transition region in the above paper). We use this model (below designated as AL) in this paper as the main one. In this model (see Table 26 and Fig. 8 in Avrett and Loeser (2008)), the heights are

measured from the base of the photosphere, from the level with the following parameters:

$$z_0 = 0\ \text{km}, \quad T_0 = 6583\ \text{K},$$
$$P_0 = 1.228 \times 10^5\ \text{dyn cm}^{-2},$$
$$n_0(H) = 1.188 \times 10^{17}\ \text{cm}^{-3}, \quad \rho_0 = 2.78\ \text{g cm}^{-3}.$$

The temperature-minimum region is located above this level, in the range of heights from 500 to 600 km: the temperature drops to $T_m = 4400$ K at a height of 560 km and only rises further out. At heights from 1300 to 2130 km, this rise is very slow: from 6600 to 6768 K. This region may be called the temperature-plateau region. A very thin transition region begins further out (we will denote its parameters by the subscript "tr"). The temperature rises to 20 000 K already at a height of 2152 km. Starting from this level, which may be taken as the boundary of the transition region, $z = z_{\text{tr}} = 2.152$ Mm, the plasma temperature rises very sharply to hundreds of thousands of kelvins and then increases monotonically up to its limiting coronal values, ~2 MK at heights of 100–200 Mm; further out, the coronal temperature ceases to rise.

Our objective in this section is to approximate the vertical temperature profile specified by the semi-empirical AL model by fairly simple analytical formulas as accurately as possible and then to obtain the corresponding profiles $P_{\text{ex}}(z)$ and $\rho_{\text{ex}}(z)$ also in the form of analytical formulas using the hydrostatic equilibrium condition for the external medium

$$\frac{dP_{\text{ex}}(z)}{dz} = -\rho_{\text{ex}}(z)g \tag{13}$$

and the equation of state for an ideal gas (6).

It is natural to divide the entire region of space to be described into three layers.

(1) The subphotospheric layers, heights $-0.5 < z < 0$. Here and below, we will measure the heights in Mm. These depths are sufficient to describe in detail the subphotospheric layers of sunspots and the footpoints of chromospheric and coronal loops buried in the photosphere.

(2) The photosphere and chromosphere, heights from $z = 0$ to $z_{\text{tr}} = 2.152$ Mm.

(3) The corona, $z > 2.152$ Mm.

We will begin with the layer adjacent to the photosphere from below, with heights from −0.500 Mm to zero. In this layer, the AL model gives a description of the medium only to a depth of 100 km. For deeper layers, we will adopt a monotonic change in temperature with depth taken from the convection zone model of Stix (2004), which is close to the AL model profile in the region of overlap between the models (-0.1 Mm $< z < 0$ Mm). The temperature curve at these depth is well approximated by the formula

$$T_{\text{ex}}(z) = \frac{6.583}{1 - 1.2(z^2)^{\frac{1}{4}} - 0.78z}, \tag{14}$$
$$-0.5 < z < 0.$$

The temperature here and below is given in thousands of K. The corresponding pressure and density profiles in the subphotospheric region are

$$\left.\begin{aligned} P_{\text{ex}}(z) &= P_0 \exp\frac{\left(-z+0.8(z^2)^{\frac{3}{4}}-0.39z^2\right)}{H_0}, \\ \rho_{\text{ex}}(z) &= \rho_0(1 - 1.2(z^2)^{\frac{1}{4}} - 0.78z) \\ &\times \exp\frac{\left(-z+0.8(z^2)^{\frac{3}{4}}-0.39z^2\right)}{H_0}, \end{aligned}\right\} \tag{15}$$
$$-0.5 < z < 0.$$

Here, $H_0 = \Re T_0(\mu g)^{-1} = 0.156$ is the local scale height at $z = 0$ expressed in Mm.

According to the AL model, the vertical temperature profile in the photosphere and chromosphere has a fairly complex shape. Let us choose the following approximation formula for it:

$$T_{\text{ex}}(z) \tag{16}$$
$$= \frac{6.583}{1 + \frac{0.71\sqrt{z}}{1+\left(1.5z^{\frac{3}{2}}\right)^6} - 0.01z - 3.4 \times 10^{-34}z^{100}},$$
$$0 < z < 2.152.$$

Here, the second term in the denominator of the fraction describes the decrease in temperature from its photospheric values to 4400 K at a level of 0.56 Mm and its return to 6600 K at a level of ~1.3 Mm. The third small term provides a slight temperature rise in the temperature-plateau region. Finally, the last term with a very high power of z describes the sharp rise in temperature as the transition region is approached: in the narrow range from 2.13 to 2.152 Mm, the temperature rises from 6800 to 20 000 K (Fig. 1). Note that we choose the temperature profile for the subsequent integration of the hydrostatic equilibrium equation (13). Therefore, when writing Eq. (16), we separated out the characteristic argument $1.5z^{\frac{3}{2}}$ in it. Since the last term in the denominator of Eq. (16) makes a very small (<1%) contribution to the pressure and density profiles, below we will discard it. Equation (13), given (6) in the photospheric–chromospheric layer under consideration, should be integrated by taking into account the fact that the mean molar mass μ changes appreciably with height from 1.288 at the photospheric level to a coronal value of 0.6 at $z = 2.152$. The reason for this decrease has to do not so much with the hydrogen ionization caused by a

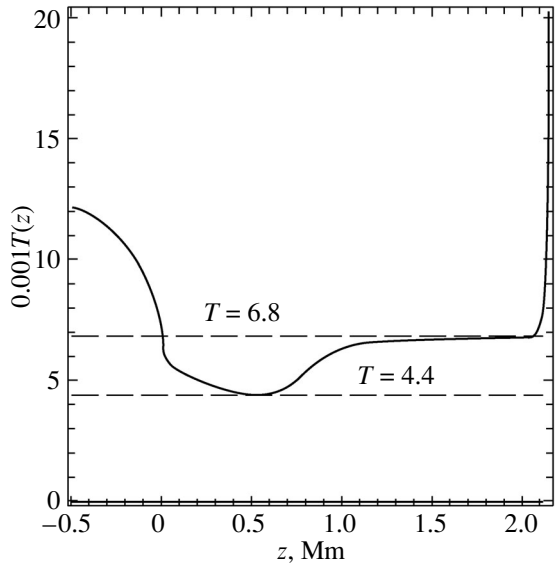

Fig. 1. The analytical dependence of temperature on height $T_{ex}(z)$ (solid line) in the range from -0.5 to 2.152 Mm calculated from Eqs. (14) and (16). The temperature is given in thousands of K, and the height z measured from the photospheric level is given in thousands of km (Mm).

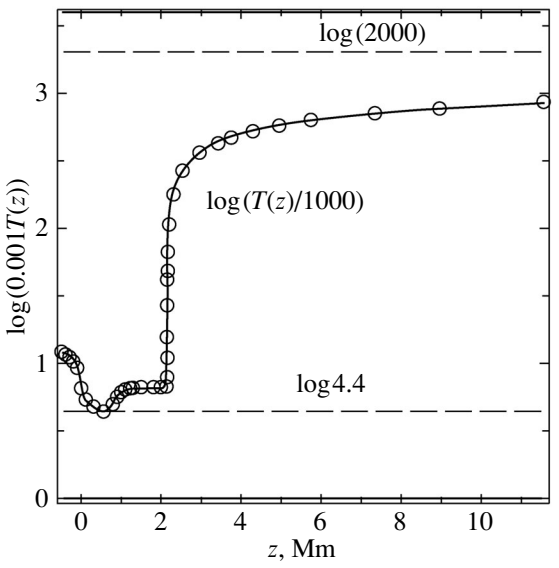

Fig. 2. The same distribution $T_{ex}(z)$ in a logarithmic form in the range from -0.5 to 11.6 Mm calculated from Eqs. (14), (16), and (19). The dashed lines mark the levels of the logarithms of minimum $0.001T_{ex}(0.56) = 4.4$ and asymptotic coronal temperature, $0.001T_c = 2000$. The circles designate the AL model data.

temperature rise as with the plasma microturbulence, which, as has been pointed out above, raises the effective pressure of the external medium. Formally, this pressure rise can be described as a decrease in the effective molar mass of the gas with height. According to the AL model, the height dependence of the effective molar mass can be represented as

$$\mu_{\text{eff}}(z) = 1.288\left[1 - 0.535\left(\frac{z}{2.152}\right)^3\right]. \qquad (17)$$

The pressure and density profiles in the chromosphere calculated by taking into account (17) will take the form

$$\left.\begin{aligned} P_{\text{ex}}(z) &= P_0\left(\frac{2.25z^3-1.5\sqrt{3}z^{\frac{3}{2}}+1}{2.25z^3+1.5\sqrt{3}z^{\frac{3}{2}}+1}\right)^{0.433} \\ &\times \exp\left(\frac{-z+0.0134z^4-0.1043F-0.0526G+0.005z^2}{H_0}\right), \\ \rho_{\text{ex}}(z) &= \rho_0\frac{P_{\text{ex}}(z)}{P_0}\left(\frac{1+0.71\sqrt{z}}{1+(1.5z^{\frac{3}{2}})^6} - 0.01z\right) \\ &\times \left(1 - \frac{0.535z^3}{(2.152)^3}\right), \end{aligned}\right\} \qquad (18)$$

$$0 < z < 2.152.$$

Here, $F = \arctan(1.5z^{\frac{3}{2}})$ and $G = \arctan(3z^{\frac{3}{2}} + \sqrt{3}) + \arctan(3z^{\frac{3}{2}} - \sqrt{3})$. The small terms making a contribution <1% are discarded in Eqs. (18).

At heights above the transition region, at $z > z_{\text{tr}} = 2.152$ Mm, the change in temperature with height can be well represented by the formula (Fig. 2)

$$T_{\text{ex}}(z) = T_c\frac{4.2a + \sqrt{z-2.152}}{4.2 + \sqrt{z-2.152}}, \quad z > 2.152. \qquad (19)$$

Here, $a = \dfrac{T_{\text{tr}}}{T_c}$, where T_c is the asymptotic coronal temperature, for which we will take $T_c = 2\times10^6$ K; thus, $a = \dfrac{20\,000}{2\times10^6} = 0.01$. In the corona, $\mu = \mu_c = 0.6$ g/mol. Under our assumptions, the hydrostatic equilibrium condition (13) and the equation of state for an ideal gas (6) lead to the following expressions for the pressure and density in the corona:

$$\left.\begin{aligned} P_{\text{ex}}(z) &= P_{\text{tr}}(\sqrt{z-2.152} + 4.2a)^{\frac{4.2a}{101}} \\ &\times \exp\left(-\frac{z-2.152+8.4\sqrt{z-2.152}}{H_c}\right), \\ \rho_{\text{ex}}(z) &= \rho_{\text{tr}}\frac{P_{\text{ex}}(z)}{P_{\text{tr}}}a\frac{4.2+\sqrt{z-2.152}}{4.2a+\sqrt{z-2.152}}, \end{aligned}\right\} \qquad (20)$$

$$z > 2.152.$$

Here, according to the AL model, $P_{\text{tr}} = 0.1056$ dyn cm^{-2}, $\rho_{\text{tr}} = 2.27\times10^{-14}$ g cm^{-3}, and $H_c = \Re T_c(\mu_c g)^{-1} = 101$ is the scale height in the corona at $T_c = 2\times\ 10^6$ K expressed in Mm, and we took into account the fact that $P_{\text{ex}}(2.152) \equiv P_{\text{tr}} = a\rho_{\text{tr}}gH_c$. Note that the scale heights H_0 and H_c differ by three orders of magnitude!

Figure 2 presents the temperature distributions calculated from Eqs. (14), (16), and (19). As can be

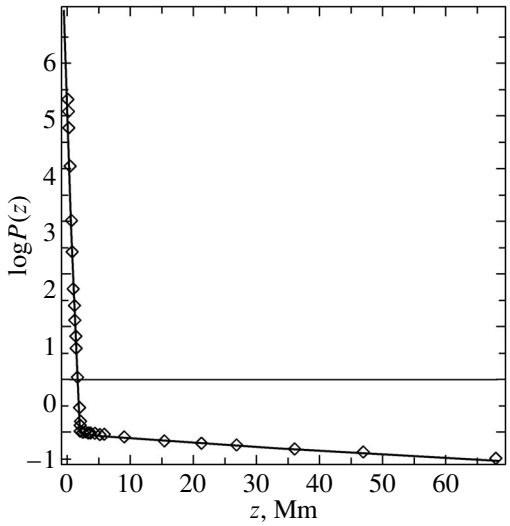

Fig. 3. Change of the logarithm of pressure $P_{ex}(z)$ expressed in 1 dyn cm^{-2} with height. The diamonds represent the AL model data.

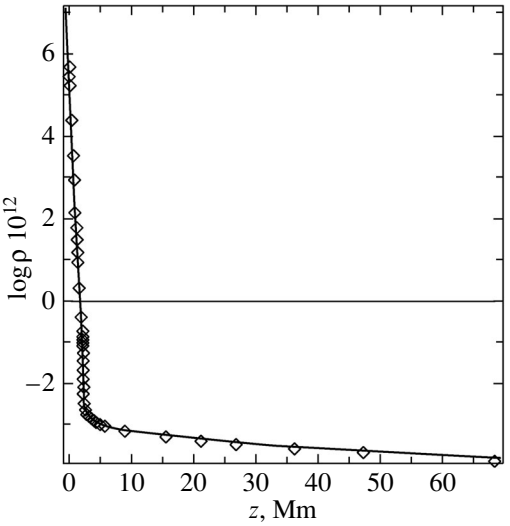

Fig. 4. Change of the logarithm of solar-atmosphere plasma density expressed in 10^{-12} g cm^{-2} with height. The diamonds represent the AL model data.

seen, these analytical formulas approximate the temperature profile of the AL model with a high accuracy. In Avrett and Loeser (2008), attention was focused on the temperature distribution that was chosen to achieve the closest correspondence of the theoretical line profiles (especially in the ultraviolet) to the observed ones. The AL temperature profile appears to have been determined fairly reliably and is close to the real one. Figures 3 and 4 show the hydrostatic vertical pressure and density distributions also in comparison with the AL data.

The fairly simple analytical model of a hydrostatic solar atmosphere constructed here in a large range of heights, from subphotospheric layers to tens of Mm in the corona, is definitely more realistic than the elementary barometric distributions commonly used in such problems. Its practical application for numerical simulations of magnetic configurations in the solar atmosphere is considerably more convenient and economical than the direct use of several hundred tabulated AL model data.

Thus, when a model of the external medium is available, the problem of determining the pressure and temperature–density distributions in an equilibrium vertical flux tube with a specified magnetic structure turns out to be completely solved in an analytical form.

5. THE MAGNETIC STRUCTURE OF A VERTICAL FLUX TUBE

As an example of using the general formulas of the magnetohydrostatic theory developed above, let us choose a vertical magnetic flux tube inside which the initial field distribution is described by the force-free solution from Schatzman (1965):

$$\left.\begin{aligned} B_z(r,z) &= B_0 J_0(kr)\exp(-lz),\\ B_r(r,z) &= \tfrac{l}{k} B_0 J_1(kr)\exp(-lz),\\ B_\varphi(r,z) &= \sqrt{1-\tfrac{l^2}{k^2}}\,B_0 J_1(kr)\exp(-lz). \end{aligned}\right\} \quad (21)$$

Here, B_0 is the magnetic field strength at the coordinate origin, $J_0(kr)$ and $J_1(kr)$ are Bessel functions of the zeroth and first orders, respectively. Solution (21) belongs to the class of linear force-free fields satisfying the condition $[\nabla\times\mathbf{B}]=\alpha\mathbf{B}$, $\alpha=\mathrm{const}$. In our case, $\alpha = k\sqrt{1-\dfrac{l^2}{k^2}}$. The linear force-free magnetic fields are remarkable in that they correspond to the minimum of magnetic energy at fixed magnetic helicity (Woltjer 1958). The magnetic flux function for (21) is

$$A(r,z) = \frac{B_0}{k^2} krJ_1(kr)\exp(-lz); \quad (22)$$

the current (or field twisting) function is proportional to the magnetic flux: $\Omega(A)=\alpha A(r,z)$. Obviously, $l\le k$, i.e., the vertical scale dominates over the horizontal one, which exactly corresponds to the structure of coronal loops. The special case of $l=k$ and $\alpha=0$ corresponds to a potential field. Any of the zeros of the Bessel function $J_1(kr_i)=0$, i.e., $R=r_i$, may be taken as the side boundary of the magnetic flux tube (21), $r=R$, because the radial and azimuthal fields become zero on such a surface, and only the vertical field enters into the boundary condition of continuity for the total pressure. (The boundary

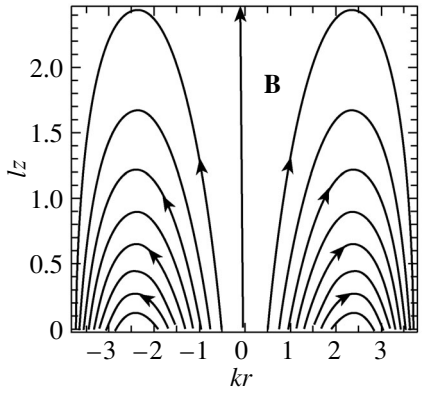

Fig. 5. Vertical section of the magnetic flux tube (21) obtained from the condition $A(r,z) = \frac{B_0}{k} r J_1(kr)\exp(-lz) = \text{const}$ at $l = 0.9k$. The azimuthal field whose field lines wrap around the z axis is not shown here.

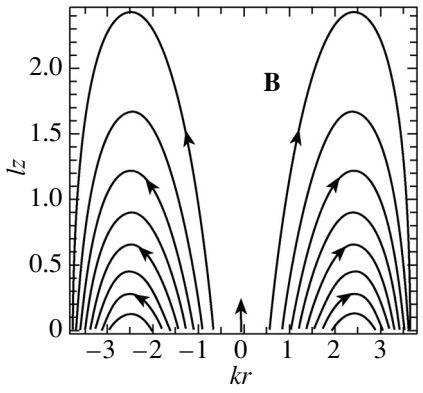

Fig. 6. Vertical section of the magnetic configuration with the modified flux function $A(r,z) = \frac{B_0}{k^{0.8}} r^{1.2} J_1(kr)\exp(-lz) = \text{const}$ at $l = 0.9k$. In this case, there is no magnetic field on the $r = 0$ axis, corresponding to the configuration of a horizontal magnetic ring in Fig. 12.

conditions and the structure of the external field are discussed below in a separate section). According to what has been said, the product kR can be one of the terms of the sequence

$$kR_i = 3.8317;\ 7.0166;\ 10.1735;\ 13.3237;$$
$$16.4706;\ 19.6158;\ 22.7601;\ 25.9037....$$

In this paper, we will restrict ourselves to the case of $i = 1$, $kR_1 = 3.8317$, although fairly large numbers i can be of interest for the problem of magnetic field concentration to the vertical-rope axis, but we will not consider these effects here. The vertical section of the magnetic flux tube (23) is presented in Fig. 5.

We will emphasize that the cross-sectional radius of the magnetic flux tube under consideration does not change with height due to the separation of variables in Eqs. (21), which is a characteristic feature of coronal loops. Note in passing that the problem of constancy of the coronal loop cross section is easily solved for magnetic loops comprising a magnetic arcade (translational symmetry). In this case, however, not the arcade but a solitary magnetic flux tube is considered.

Potential and force-free magnetic fields do not perturb the hydrostatic state of the medium in which they are immersed, because the magnetic force in these fields becomes zero. Consequently, purely potential or force-free magnetic structures cannot be observed in principle in the solar atmosphere. For them to be "visible," observable, some deviations from the force-free (or potential) state must appear in the corresponding field distributions. One of such deviations can be an excess or reduction of the magnetic field twisting compared to its force-free level. Let the azimuthal component of distribution (21) be

$$B_\varphi(r,z) = b\sqrt{1 - \frac{l^2}{k^2}} B_0 J_1(kr)\exp(-lz), \quad (23)$$

where b is some positive coefficient of the order of unity. There is the initial force-free state (21) at $b = 1$; the equilibrium magnetic structure at $b \neq 1$ is no longer a force-free one; the gas pressure, density, and temperature distributions inside such a tube differ from the hydrostatic distribution of the external medium.

What is remarkable in this case is that, as it has turned out, the sign of this deviation is directly related to the sign of the difference $b - 1$. If this difference is positive, i.e., $b > 1$, then the additions to the pressure and density attributable to the magnetic field are also positive in the entire tube volume. Otherwise, when $b < 1$, i.e., the field twisting turns out to be below the force-free level, the additions to the pressure and density profiles in the tube become negative; at a sufficiently large deviation from the force-free state, the resulting pressure and/or density at some points of the magnetic flux tube may turn out to be arbitrarily small, close to zero. As the field twisting b decreases further, these quantities formally become negative, which has no physical meaning. This simply means that a configuration with such parameters cannot be balanced in a given hydrostatic medium at a given geometric level. To return the system to the region of equilibrium states, we should change (reduce) the unit of measurement of the magnetic field B_0, i.e., increase the plasma parameter $\beta_0 = 8\pi P_{\text{ex}}(0) B_0^{-1}$ or choose a twisting coefficient b to be not too small compared to unity. The aforesaid is illustrated graph-

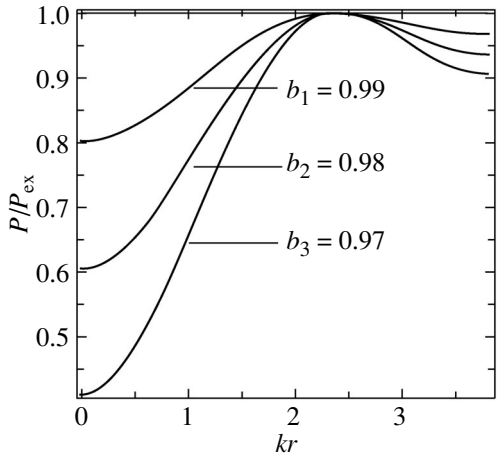

Fig. 7. Radial pressure profile in a vertical flux tube at $z = 0$ (in units of the background pressure) at $l^2 = 0.9k^2$ and $b_1 = 0.99$, $b_2 = 0.98$, $b_3 = 0.97$. The gas pressure was reduced through a reduction in twisting compared to the force-free level.

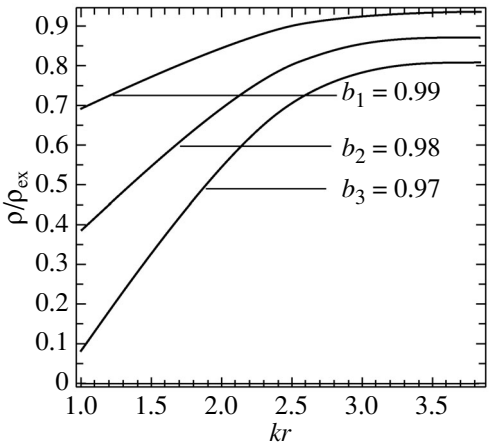

Fig. 9. Radial density profile in a vertical flux tube at $z = 0$ (in units of the background density) at $l^2 = 0.9k^2$ and $b_1 = 0.99$, $b_2 = 0.98$, $b_3 = 0.97$. The gas density in the rope is reduced through a decrease in twisting compared to its force-free level.

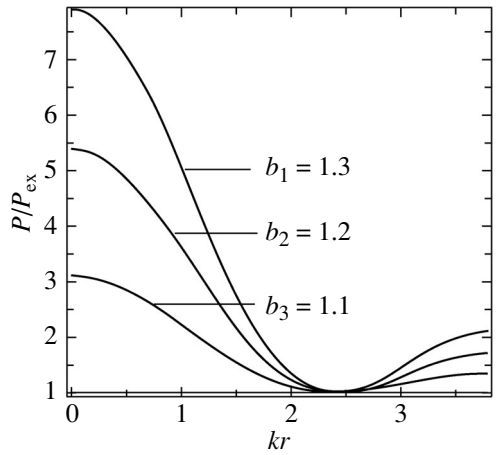

Fig. 8. Radial pressure profile in a vertical flux tube at $z = 0$ (in units of the background pressure) at $l^2 = 0.9k^2$ and $b_1 = 1.3$, $b_2 = 1.2$, $b_3 = 1.1$. The gas pressure is enhanced through an increase in twisting compared to the force-free level.

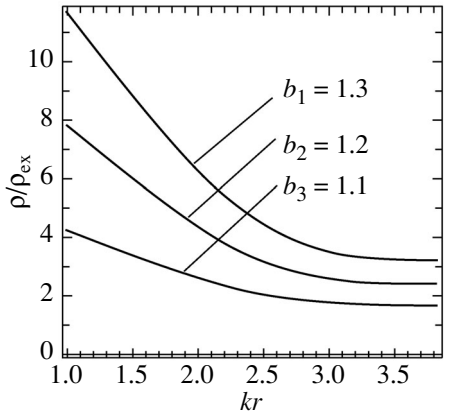

Fig. 10. Radial density profile in a vertical flux tube at $z = 0$ (in units of the background density) at $l^2 = 0.9k^2$ and $b_1 = 1.3$, $b_2 = 1.2$, $b_3 = 1.1$. The gas density in the magnetic flux tube is enhanced owing to an increase in field twisting compared to its force-free level.

ically in Figs. 7, 8 and 9, 10 with several numerical examples.

6. THE MECHANISM OF ENERGY RELEASE IN MAGNETIC FLUX ROPES

The energy release in solar flares is usually attributed to the reconnection of magnetic field lines in large-scale current sheets (Syrovatskii 1981; Priest 1985; Priest and Forbes 2000). For example, the "standard" flare model (Sturrock 1968; Kopp and Pneuman 1976; Tsuneta 1997; Shibata 2005; Shibata and Magara 2011; etc.) suggests the formation of a vertical current sheet beneath the lower outline of a twisted magnetic loop (rope) rising into the corona through the deformation by this loop of the external magnetic field transverse to it. The magnetic flux rope acts here as a driver of the entire flare process. In several cases, this model seems fairly adequate to the observed phenomena. However, more and more observational evidence that intense flare energy release occurs more often in low-lying helically twisted loops (sigmoids) without any apparent signs of large-scale reconnection has appeared in recent years (see, e.g., Aschwanden 2014).

For example, in the July 6, 2011 flare event, a powerful CME in the form of a twisted magnetic loop that carried away a very large amount of cold chromo-

spheric material into the corona occurred first. Only laminar flows of dark material dragged upward in the wake of the rising rope were observed under this magnetic loop that flew out into the corona and subsequently into the heliosphere, but no current sheet was formed beneath the loop—this is clearly seen in the images and videos obtained by the AIA (Atmospheric Imaging Assembly) instrument of the Solar Dynamic Observatory (SDO). Another twisted flux rope with the same spatial orientation as that of the first one went into the chromosphere at the same place after the CME, but it was not ejected into the corona, remaining at heights near the transition region, and violent energy release that lasted about 1.5 h began in it. This event was interpreted by Solov'ev (2012) within the framework of an exact magnetostatic solution for two quasi-parallel magnetic flux ropes that emerged successively and relatively slowly, quasi-statically, from beneath the photosphere. According to the solution found, the plasma density in the first (upper) rope was enhanced significantly compared to the surrounding medium; therefore, no flare energy release would be possible in it, and this filament was vigorously ejected into the corona due to large field twisting, carrying away a considerable excess of mass. In contrast, according to the derived quasi-static distribution, the plasma density in the second, subsequently emerged magnetic flux rope was reduced considerably with respect to the coronal one. As a result, the electron drift velocity in this rope turned out to be high enough for plasma kinetic instabilities to be excited in it, and the free energy of the azimuthal magnetic field served here not as a driver of the mechanical ejection but as a source of the observed flare energy release. In other words, the store of free energy was converted in this rope not into the kinetic and potential energy of the ejection but into the energy of accelerated nonthermal particles, into ultraviolet and soft X-ray plasma radiation, and into an increase in the total bolometric luminosity of the filament.

A second example of such a kind was the X1 flare that occurred on September 22, 2011, and lasted about 12 h. Here, a characteristic feature of the event was the prolonged sucking of cold chromospheric material from the surrounding medium directly into the hot region of flare energy release located low in the chromosphere. The pattern of motion of the material drawn into the flare region along a low helical trajectory clearly pointed to a significant twisting of the magnetic flux rope in which the energy release occurred. As in the previous case, the model of this event (Solov'ev and Murawski 2014) was based on the idea that when the magnetic flux rope goes into the rarefied layers of the solar atmosphere, the requirement of a transverse equilibrium of the magnetic flux tube can lead to a sharp decrease in the plasma pressure and density in some region inside the rope. Given a certain electric current density in the rope that is required by the condition of equilibrium of a twisted flux tube, the electron drift velocity $V_{e,dr}$ in this place will increase sharply, and the excitation of plasma oscillations (in particular, ion sound) will begin in the plasma when it approaches the thermal ion velocity, $V_{th,i} = \sqrt{2kTM_i^{-1}}$. This will lead to a considerable scattering of electrons by plasmons and to the appearance of anomalous plasma resistivity, with all the ensuing consequences. The sequence of elementary formulas given below explains the aforesaid:

$$\mathbf{j} = \frac{c}{4\pi}[\nabla \times \mathbf{B}] \approx \text{const} \Rightarrow j = n_e e V_{e,dr} \qquad (24)$$

$$\approx \text{const} \Rightarrow V_{e,dr} = \frac{\text{const}}{n} \Rightarrow V_{dr} = V_{th,i}\frac{n_{cr}}{n},$$

$$\text{where} \quad V_{th,i} = \sqrt{\frac{2kT}{M_i}}.$$

The main idea of our approach is that the flare energy release in twisted magnetic flux ropes (sigmoids) is attributable to the excitation of plasma instabilities in them (Bernstein modes, ion sound) caused by a sharp drop in the plasma density in some region inside the rope that arises in it when an equilibrium is established as the rope emerges from beneath the photosphere. A shortage of charge carriers in some plasma volume at a fixed electric current density increases their drift velocity, and conditions for the excitation of plasma turbulence are created in this place when the latter approaches the thermal ion velocity. Thus, in the context of this ideology, the twisting of the rope magnetic field (and the corresponding free magnetic energy of the electric currents) serves as a source of the energetics of a chromospheric flare.

7. THE MODEL OF A RING FLARE FILAMENT

In this paper, we would like to develop the same idea of the excitation of plasma turbulence in a rarefied magnetic filament as applied to yet another case of a flare event observed by the TRACE spacecraft in 2000. Figure 11 shows six successive images of a horizontal flare filament in the chromosphere that had the shape of an almost regular ring.

A schematic view of the horizontal ring corresponding in its geometry to the described flare configuration with a magnetic field twisted around its toroidal axis is presented in Fig. 12.

To describe the magnetic field of such a ring configuration, we use a magnetic flux function slightly

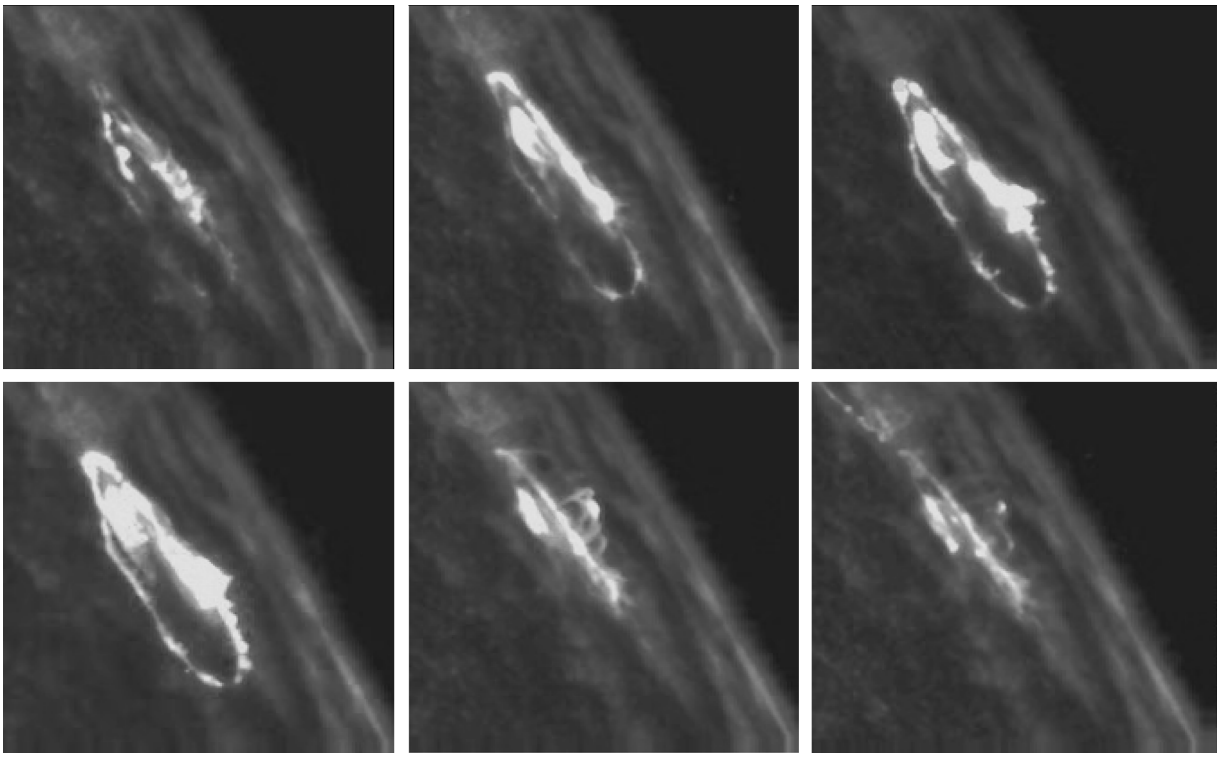

Fig. 11. Successive stages of the propagation of flare excitation in a ring magnetic structure. The last frame (bottom right) shows how another slightly fainter ring ignites in the upper left corner of this frame.

different from (22) to ensure the absence of a magnetic field on the symmetry axis of the ring, at its center:

$$A(r,z)=\frac{B_0}{k^2}(kr)^m J_1(kr)\exp(-lz), \qquad (25)$$

where m is a positive constant greater than one. In this case, according to (7),

$$B_z(r,z)=B_0\Big[(kr)^{m-1}J_0(kr) \qquad (26)$$

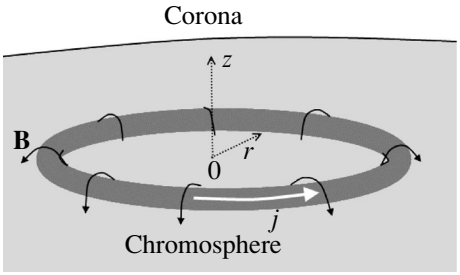

Fig. 12. Horizontal flare filament in the solar chromosphere. The solid black lines indicate the field lines of magnetic field **B**, the white arrow indicates the direction of the electric current in the filament, and the thin dotted lines represent the cylindrical coordinate system.

$$+(m-1)(kr)^{m-2}J_1(kr)\Big]\exp(-lz)$$

and $B_z(0,z)=0$. We will choose $m=1.2$ for a numerical example. The vertical section of such a magnetic structure is shown in Fig. 6. For the azimuthal field, we will take the same Eq. (25) with a coefficient b different from unity. Of course, this doubly "corrected" field compared to (21) will no longer be a force-free one; deviations in the pressure and density profiles from the background hydrostatic distributions will appear. These profiles follow the same trends as those for a rope with the magnetic flux (22): as the twisting increases, at $b>1$, the additions to the pressure and density are positive, while as the twisting decreases, at $b<1$, these additions turn out to be negative at a certain distance from the axis. Numerical examples are given in Figs. 13 and 14. It can be seen from them that the gas pressure at the chosen configuration parameters is everywhere positive, but the gas density in the area near $kr=1.5$ becomes arbitrarily small if the twisting parameter b approaches 0.829. This result was obtained at $m=1.2$ and $l^2=0.1k^2$.

We can choose other values of these parameters for the system, but the main result is retained: we can always choose such a twisting $b<1$ that the

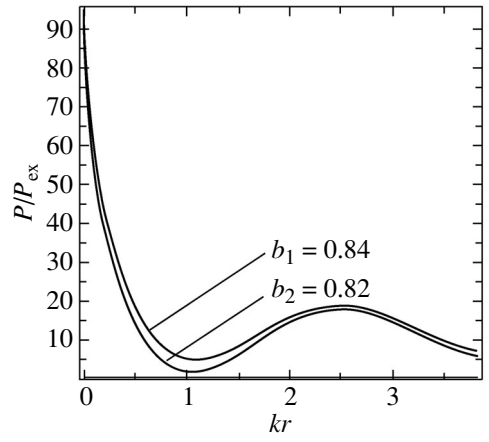

Fig. 13. Radial pressure profile in a horizontal circular filament at $z = 0$ (in units of the background pressure) at $m = 1.2$, $l^2 = 0.1k^2$ and $b_1 = 0.84$, $b_3 = 0.82$. The pressure remains constant at all points.

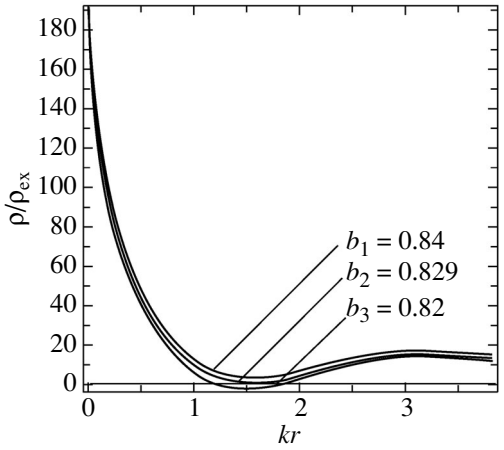

Fig. 14. Radial plasma density profile in a horizontal ring at $z = 0$ (in units of the density of the external medium) at $m = 1.2$, $l^2 = 0.1k^2$ and $b_1 = 0.84$, $b_2 = 0.829$, and $b_3 = 0.82$. For $b \to b_2 = 0.829$ the plasma density at a distance $kr \approx 1.5$ approaches zero, while at $b = b_3 = 0.82$ it turns out to be negative at this point.

equilibrium gas density at some distance from the axis will approach zero. For example, if we take $m = 1.1$ and $l^2 = 0.8k^2$, then the gas density will become zero at $kr = 1.55$ at $b = 0.59$.

This effect of a reduction in density with decreasing field twisting is of fundamental importance for the rope mechanism of energy release we discuss. Indeed, if the effect had the opposite sign, i.e., if the density increased with decreasing field twisting, then the energy release based on the excitation of plasma turbulence would decay as soon as it began: the decrease in field twisting due to current dissipation on anomalous resistivity would cause an increase in density, i.e., an increase in the number of charge carriers and a decrease in the electron drift velocity below the excitation threshold.

In our case, the situation is completely different. Once begun, the electric current dissipation in the rope leads to a decrease in density and a further increase in drift velocity in the rarefaction region, i.e., the entire process acquires the irreversible pattern of catastrophically rapid conversion of the free magnetic energy of electric currents into the energy of accelerated particles, radiation, and heating of the surrounding plasma.

8. THE EQUILIBRIUM BOUNDARY CONDITIONS

As has been said in Section 5, we choose the surface with the radial coordinate $kr = kR_1 = 3.8317$ as the side boundary surface of our configuration. On this surface $J_1(kR_1) = 0$, i.e., the azimuthal and radial components become zero, while the longitudinal field is $B_z(R, z) = B_0(kR)^{m-1}J_0(kR)\exp(-lz) = -0.523B_0\exp(-lz)$ if $m = 1.2$. If $m = 1$, then $B_z(R, z) = -0.4B_0\exp(-lz)$.

To describe the field in the external region, we can take, for example, the following flux function:

$$A(r, z) = B_0^{ex}R^2\left[\frac{R}{r} - 1\right]\exp(-lz), \qquad (27)$$
$$\Omega(A) = 0, \quad r > R.$$

The magnetic field configuration outside of the flux tube under consideration is

$$\left.\begin{aligned} B_z(r, z) &= -B_0^{ex}\tfrac{R^3}{r^3}\exp(-lz), \\ B_r(r, z) &= B_0^{ex}Rl\tfrac{R}{r}\left[\tfrac{R}{r} - 1\right]\exp(-lz), \\ B_\varphi(r, z) &= 0, \end{aligned}\right\} \qquad (28)$$
$$r > R.$$

To fulfil the condition of continuity for the magnetic pressure at the boundary, it will suffice to assume that $B_0^{\rm ex} = 0.523B_0$ or $0.4B_0$ for $n = 1$. The situation with the gas pressure continuity at the boundary is slightly more complex. According to Eq. (8), the expression for the pressure contains the integral term $\frac{1}{4\pi}\int_r^\infty \frac{\Omega^2}{r^3}dr$ that does not become zero at the boundary $r = R$, and, as a consequence, $P(R, z)$ depends on the field twisting in the rope (see Figs. 7 and 8). There is no azimuthal field outside of the magnetic flux tube, and, hence, $P_{\rm ex}(R, z)$ does not depend on the field twisting here. The gas pressure continuity at the boundary can be ensured by small

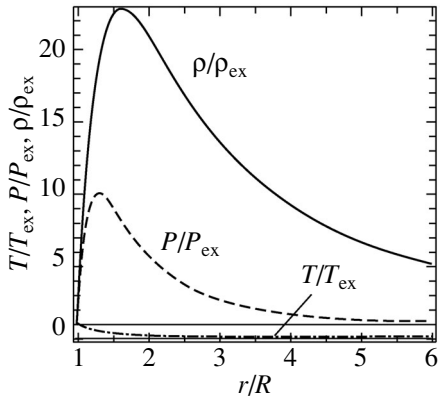

Fig. 15. Radial plasma pressure, density, and temperature distributions outside ($r > R$) of the magnetic flux tube corresponding to the magnetic field (28) at $(Rl)^2 = 6$ and $\beta_0 = \dfrac{8\pi P_{\rm ex}(0)}{B_0} = 0.01$.

variations of the product Rl, on which no conditions are imposed in the external medium. The most important fact here is that the density and pressure deviations from the hydrostatic background caused by the external magnetic field must be positive in the entire outer space. Figure 15 presents the pressure, density, and temperature distributions outside of the tube at $(Rl)^2 = 6$. No problems with negative pressure, density, and temperature arise in this case. At the boundary, at $r = R$, all these three quantities are equal to the external background values, consistent with the force-free distribution inside the magnetic flux tube ($b = 1$). When $(Rl)^2$ deviates from 6, they can be above or below this level, depending on the field twisting inside the rope, i.e., on the factor b, to ensure the gas pressure continuity at the boundary.

9. CONCLUSIONS

A closed magnetostatic theory of a vertical magnetic flux tube immersed in a realistic solar atmosphere was presented in an analytical form. Its specific applications to modeling the vertical parts of coronal loops with a constant cross section whose tops are located high in the corona and to the description of horizontal flare filaments were considered. The mechanism of flare energy release in a twisted magnetic flux tube is reduced to the fact that with its exit into the chromosphere, as a new equilibrium is established in it, the concentration of particles corresponding to this equilibrium decreases to vanishingly small values in some part of its volume, despite the fact that the electric current density here is nonzero and remains constant according to the equilibrium conditions: $\mathbf{j} = c(4\pi)^{-1}\mathrm{curl}\mathbf{B}; j = n_e e V_{e,dr} \approx \mathrm{const}$. In such a situation, the electron drift velocity in the rarefied region, where $n \to 0$, will grow sharply as the loop rises upward, reaching the thermal ion velocity. This leads to the instantaneous excitation of plasma instabilities (Bernstein modes, ion sound), the appearance of "anomalous" resistivity, runaway particles, i.e., in essence, to a solar flare.

Thus, the proposed flare model does not deal with the traditional mechanism of magnetic field line reconnection in the solar corona. We suggest that a fairly strong twisting of the magnetic field and a high degree of nonuniformity of the equilibrium gas density distribution over the volume of the magnetic flux rope are responsible for the flare energy release in rope magnetic configurations.

ACKNOWLEDGMENTS

This work was supported by Program P-09 of the Presidium of the Russian Academy of Sciences and the Russian Foundation for Basic Research (project no. 13-02-00714).

REFERENCES

1. M. J. Aschwanden, in *Proceedings of the American Astronomical Society Meeting No. 224, June 1–5, 2014, Boston, MA* (AAS, 2014), Abstract No. 123.6.
2. E. H. Avrett and R. Loeser, Astrophys. J. Suppl. Ser. **175**, 229 (2008).
3. F. A. Gent, V. Fedun, and R. Erdelyi, Astrophys. J. **789**, 42 (2014).
4. H. Grad, Rev. Mod. Phys. **32**, 830 (1960).
5. R. A. Kopp and G. W. Pneuman, Solar Phys. **50**, 85 (1976).
6. B. C. Low, Astrophys. J. **197**, 251 (1975).
7. B. C. Low, Solar Phys. **67**, 57 (1980).
8. B. C. Low, Astrophys. J. **263**, 952 (1982).
9. B. C. Low, Astrophys. J. **293**, 31 (1985).
10. V. N. Obridko and A. A. Solov'ev, Astron. Rep. **55**, 1144 (2011).
11. E. N. Parker, *Cosmical Magnetic Fields* (Clarendon Press, Oxford, 1979), Part 1.
12. E. R. Priest, *Solar Magnetohydrodynamics* (Reidel, London, 1982).
13. E. N. Priest and T. Forbes, *Magnetic Reconnection. MHD Theory and Applications* (Cambridge Univ. Press, 2000).
14. E. Schatzman, IAU Symp. **22**, 337 (1965).
15. V. D. Shafranov, Sov. Phys. JETP **6**, 545 (1957).
16. V. N. Shapovalov and O. V. Shapovalova, Russ. Phys. J. **46**, 186 (2003).
17. K. Shibata, IAU Symp. **226**, 241 (2005).
18. K. Shibata and T. Magara, Living Rev. Solar Phys. **8**, 6 (2011).
19. A. A. Solov'ev, Astron. Rep. **54**, 86 (2010).

20. A. A. Solov'ev and E. A. Kirichek, Astron. Lett. **37**, 791 (2011).
21. A. A. Solov'ev, Geomagn. Aeron. **52**, 1062 (2012).
22. A. A. Solov'ev, Solar Phys. **286**, 441 (2013).
23. A. A. Solov'ev and K. Murawski, Astrophys. Space Sci. **350**, 11 (2014).
24. A. A. Solov'ev and E. A. Kirichek, Astrophys. Space Sci. **352**, 23 (2014).
25. H. C. Spruit, Solar Phys. **34**, 277 (1974).
26. M. Stix, *The Sun: An Introduction, 2nd ed.* (Springer, Berlin, 2004).
27. P. A. Sturrock, IAU Symp. **35**, 471S (1968).
28. S. I. Syrovatskii, Ann. Rev. Astron. Astrophys. **19**, 163 (1981).
29. K. C. Tsinganos, Astrophys. J. **245**, 764 (1981).
30. S. Tsuneta, Astrophys. J. **483**, 507 (1997).
31. J. E. Vernazza, E. H. Avrett, and R. Loeser, Astrophys. J. Suppl. Ser. **45**, 635 (1981).
32. L. Woltjer, Proc. Natl. Acad. Sci. **44**, 489 (1958).

Translated by V. Astakhov